Received: 2 February 2022 | Revised: 9 May 2022 | Accepted: 12 May 2022

DOI: 10.1111/cas.15434

ORIGINAL ARTICLE

Cancer Science WILEY

A single immunization with cellular vaccine confers dual protection against SARS-CoV-2 and cancer

Kanako Shimizu[1] | Shogo Ueda[1] | Masami Kawamura[1] | Mikiko Satoh[1] | Shin-ichiro Fujii[1,2]

[1]Laboratory for Immunotherapy, RIKEN Center for Integrative Medical Science, Yokohama, Kanagawa, Japan

[2]Program for Drug Discovery and Medical Technology Platforms, RIKEN, Yokohama, Kanagawa, Japan

Correspondence
Shin-ichiro Fujii, Laboratory for Immunotherapy, RIKEN Research Center for Integrative Medicine (IMS), Yokohama, Kanagawa 230-0045, Japan.
Email: shin-ichiro.fujii@riken.jp

Funding information
Japan Society for the Promotion of Science, (Grant/Award Number: '19 K07653') RIKEN DMP program.

Abstract

The efficacy of current coronavirus disease 2019 (COVID-19) vaccines has been demonstrated; however, emerging evidence suggests insufficient protection in certain immunocompromised cancer patients. We previously developed a cell-based anticancer vaccine platform involving artificial adjuvant vector cells (aAVCs) capable of inducing a strong adaptive response by enhancing the innate immunity. aAVCs are target antigen-transfected allogenic cells that simultaneously express the natural killer T-cell ligand–CD1d complex on their surface. In the present study, we applied this system for targeting the severe acute respiratory syndrome coronavirus 2 (SARS-CoV-2) spike protein (CoV-2-S) using CoV-2-S-expressing aAVCs (aAVC-CoV-2) and evaluated the immune response in a murine model. A single dose of aAVC-CoV-2 induced a large amount of CoV-2-S-specific, multifunctional CTLs in addition to $CD4^+$ T-cell-dependent anti-CoV-2-S-specific Abs. CoV-2-S-specific CTLs infiltrated the lung parenchyma and persisted as long-term memory T cells. Furthermore, we immunized mice with CoV-2-S- and tumor-associated antigen (TAA)-co-expressing aAVCs (aAVC-TAA/CoV-2) and evaluated whether the anti-SARS-CoV-2 and antitumor CTLs were elicited. We found that the aAVC-TAA/CoV-2-S therapy exerted apparent antitumor effects and induced CoV-2-S-specific CTLs. These findings suggest aAVC-TAA/CoV-2-S therapy as a promising vaccine candidate for preventing COVID-19, as well as enhancing the effectiveness of cancer therapies.

KEYWORDS
cancer, COVID-19, Cytotoxic T cells, natural killer T cells, vaccine

Abbreviations: α-GalCer, α-galactosylceramide; aAVC, artificial adjuvant vector cell; aAVC-CoV-2, SARS-CoV-2 spike protein-expressing aAVCs; aAVC-TAA, tumor-associated antigen-expressing aAVCs; aAVC-WT1, WT1-antigen-expressing aAVCs; CoV-2-S, SARS-CoV-2 spike protein; COVID-19, coronavirus disease 2019; DC, dendritic cell; HLA, human leukocyte antigen; IL, interleukin; iNKT, invariant natural killer T cell; IVT, in vitro transcription; LNP, lipid nanoparticle; MNC, mononuclear cell; NK, natural killer; OVA, ovalbumin; SARS-CoV-2, severe acute respiratory syndrome coronavirus 2; TCR, T-cell receptor; Th, T helper cell; TRP2, tyrosinase-related protein 2; WT1, Wilms' tumor 1.

1 | INTRODUCTION

The coronavirus disease 2019 (COVID-19) pandemic caused by severe acute respiratory syndrome coronavirus 2 (SARS-CoV-2) has recently been a formidable threat to humanity.[1] Several COVID-19 vaccines, including an mRNA-based vaccine- and an adenovirus-vectored vaccine expressing the SARS-CoV-2 spike protein (CoV-2-S), have been administered through global vaccination programs. Specifically, antigen-encoding nucleoside-modified mRNA encapsulated in LNPs (referred to as nucleoside-modified mRNA-LNP vaccines) have recently demonstrated significant promise and are widely accepted, showing a vaccine efficacy of ~95% in healthy subjects.[2,3] Furthermore, the benefits of the vaccine, including safety, ease of production, and scalability, have been proven. Recently, a third dose of the current vaccine has been attempted, with the number of required doses dependent on the results of a durable, protective neutralizing Ab and CTLs against SARS-CoV-2. However, even with a complete return to pre-pandemic normalcy, some challenges for high-risk groups remain to be considered.

$CD8^+$ CTLs can eliminate viruses in infected cells or latently infected cells, and their role against COVID-19 has been re-evaluated.[4–6] CTLs against SARS-CoV-2-specific epitopes, as well as cross-reactive epitopes with seasonal coronaviruses, were reportedly induced in SARS-CoV-2-infected patients and convalescents.[7–11] Notably, several studies have demonstrated that pre-existing CTLs with cross-protection against SARS-CoV-2 can expand in vivo to support rapid viral control.[5,6,12] Recently, we and other groups identified immunodominant epitopes of SARS-CoV-2 protein and reported pre-existing $CD8^+$ T cells cross-reacting with seasonal coronavirus in an HLA-dependent manner.[13–16] Additionally, we showed that pre-existing, cross-reactive CTLs generated from seasonal coronavirus respond against the CoV-2-S QYI peptide in >80% of HLA-$A24^+$ healthy donors, but only in 14% of HLA-$A24^+$ patients with hematologic malignancies.[13] By contrast, despite extremely low B-cell or Ab production, a sufficient $CD8^+$ T-cell frequency can reduce COVID-19-related mortality in hematologic malignancies.[4] Therefore, a vaccine eliciting a strong $CD8^+$ CTL response against SARS-CoV-2 is needed as another vaccine candidate for high-risk groups.

When activated by α-galactosylceramide (α-GalCer), invariant natural killer T (iNKT) cells induce DC maturation in vivo, and co-administration of protein and α-GalCer generates an antigen-specific T-cell response.[17,18] Additionally, we previously established an mRNA-transfected cell-based vaccine (the aAVC system[19–21]) that includes an antigen-derived mRNA and CD1d mRNA co-transfected, iNKT cell ligand-loaded cell-based vaccine. When administered intravenously, aAVC can activate iNKT and NK cells as an adjunct activity of iNKT cells, and after activation, innate iNKT/NK cells reject the aAVCs; however, the killed aAVCs are taken up by DCs in situ, thereby activating several DC-specific immunogenic features. In the lungs, liver, and spleen, DCs that capture aAVCs undergo maturation via interaction with iNKT cells that is brought about by CD40L/CD40 interactions and inflammatory cytokines (interferon [IFN]-γ and tumor necrosis factor [TNF]-α).[19–21] Subsequently, high-frequency of antigen-specific, IFN-γ-producing $CD8^+$ T cells can be induced by the antigen-captured mature DCs[22,23] Previous studies have reported that administration of tumor (melanoma-associated antigen recognized by T cells-1 and WT1) or influenza antigen, HA-expressing aAVCs in tumor therapeutic models or influenza-prevention infectious models induced potent $CD4^+$ and $CD8^+$ T-cell responses.[20,21,24] Moreover, following therapy, memory $CD8^+$ T cells in lymphoid and non-lymphoid tissues have been observed. Vaccination with aAVC elicits not only long-term induction of antigen-specific $CD4^+$ T helper (Th) cells but also an efficient Ab response through B-cell lymphoma-6 in $CD4^+$ T follicular helper cells. Furthermore, the HA-expressing aAVC vaccine demonstrated protection against influenza virus infection in mice.[24] Recently, we developed WT1-antigen-expressing aAVC (aAVC-WT1) therapy for humans as cancer therapeutic drugs[13] and completed the first human clinical trial of aAVC-WT1 therapy for patients with relapsed and refractory AML.

In this study, we establish CoV-2-S-antigen-expressing aAVCs (aAVC-CoV-2) and evaluated the immunological evidence of $CD4^+$ and $CD8^+$ T-cell responses through cross-priming of in vivo DCs, as well as Ab production, by aAVC-CoV-2 treatment. Furthermore, as a new vaccine model, we evaluated the potential establishment of a multivalent vaccine capable of expressing two types of different antigens (CoV-2-S plus tumor-associated antigen [TAA]) and determined its ability to simultaneously generate CTLs against the virus and tumor cells.

2 | MATERIALS AND METHODS

2.1 | Animals and cell lines

Pathogen-free C57BL/6 (B6) mice (6–8 weeks old) were purchased from Charles River Japan. B6.129S2-$H2^{dlAb1\text{-}Ea}$/J (MHC class II-KO) mice were purchased from the Jackson Laboratory. CD1d1-deficient mice[25] were provided by Dr. Luc van Kaer (Vanderbilt University Medical Center, Nashville, TN, USA). All mice were maintained under specific pathogen-free conditions and studied in compliance with institutional guidelines. The NIH3T3 cell line was obtained from the RIKEN Cell Bank. The B16 and MO4 (OVA-expressing B16 melanoma) cell line[26] was received from Dr. R. M. Steinman (The Rockefeller University). Murine NKT hybridoma, 1B6 cell line was kindly provided by Dr. Kronenberg M (La Jolla Institute).

2.2 | In vitro transcription of RNA

The OVA and human TRP2 plasmids used for this study have been described previously.[20] To clone the CoV-2-S gene (accession no. NC_045512.2), the sequence was divided into four fragments with 15 bases of homology at each end and artificially synthesized using GeneArt High-Q Strings (Thermo Fisher Scientific). The four

CoV-2-S gene fragments were inserted into the *Hin*dIII and *Eco*RI sites of the pGEM-4Z vector. Sequence analysis confirmed that the cloned sequence encoded the CoV-2-S protein. Before IVT, the CoV-2-S plasmid was linearized with *Eco*RI and purified as described. IVT was performed using the mMessage mMachine T7 Ultra kit (Ambion; Thermo Fisher Scientific) according to manufacturer's instructions. RNA was purified using the RNeasy Mini/Midi kit (Qiagen), and integrity was verified by denaturing agarose gel electrophoresis.

2.3 | Preparation of artificial adjuvant vector cells

To load α-GalCer, NIH3T3 cells were cultured for 48 h in the presence of 500 ng/ml α-GalCer (Funakoshi Co., Ltd.) and then washed three times before electroporation with antigen mRNA together with murine CD1d mRNA. RNA electroporation of NIH3T3 cells was performed as previously described.[20] Briefly, cells were resuspended in OptiMEM at a concentration of 5×10^7 cells/ml. After RNA was transferred to a cuvette (Harvard Apparatus), the cell suspension was added and pulsed in an ECM 830 square wave electroporation system (Harvard Apparatus) using a single 500-V, 3-ms square pulse. Immediately after electroporation, the cells were transferred to medium and cultured in the presence of 500 ng/ml α-GalCer. Transfected cells were analyzed via western blot for the CoV-2-S protein and flow cytometry for CD1d.

2.4 | Semi-quantitative antigen-specific IgG ELISA

The antigen-specific IgG, IgG1, and IgG2b titers in mouse sera were assessed by semi-quantitative ELISA. Sera were harvested at days 14, 28, and 56 and 6 months after immunization with aAVC-CoV-2. Mice were re-challenged with aAVC-CoV-2 at 6 months, and sera were harvested 7 days after re-challenge. MaxiSorp high-binding ELISA plates (Nunc; Thermo Fisher Scientific) were coated with 100 μl of 1 μg/ml recombinant CoV-2-S glycoprotein S1 (ab272105) or CoV-2-S glycoprotein S2 (ab272106) in PBS. To recognize standard anti-SARS-CoV-2 S1 and anti-SARS-CoV-2 S2, we used anti-SARS-CoV-2 S1 (mouse IgG2b, clone #57, 40,592-MM57; Sino Biological Inc.) and anti-SARS-CoV-2 S2 (Mouse IgG1, clone 1A9, GTX632604; GeneTex) Abs. After overnight incubation at 4°C, the plates were washed three times and blocked for 1 h at room temperature with 200 μl super blocking buffer (#37535; Thermo Fisher Scientific). The plates were then washed, and the diluted samples or a two-fold dilution series of the standard anti-SARS-CoV-2 S1 or anti-SARS-CoV-2 S2 Ab was added at 100 μl/well. Plates were incubated for 2 h at room temperature and washed, followed by the addition of the secondary Ab (1:1000) in blocking buffer (100 μl/well) using either anti-mouse HRP-conjugated IgG1 (#18–4015-82; eBioscience) or IgG2b (Cat.#M32407; Invitrogen). After incubation and washes, plates were developed using 100 μl 3,3,5,5-tetramethylbenzidine substrate (BD Biosciences), and the reaction was stopped after 5 min with 50 μl/well of 1 N H_2SO_4. Absorbance was read on an iMark microplate reader at 450 nm (Bio-Rad).

2.5 | Sample processing and flow cytometry

Mononuclear cells from the spleen and lungs of mice were isolated, as previously described.[21] Briefly, splenocytes were obtained by pressing the spleen through a 70-μm cell strainer or digested using collagenase D (Roche), and erythrocytes were lysed with ACK lysing buffer (Gibco), followed by two washes with RPMI medium. For isolation of lung MNCs, the tissues were digested with collagenase D (Roche) and then layered on Percoll gradients (40/60%; Amersham plc) and centrifuged for 20 min at 900*g*. The cells were then washed with PBS, and erythrocytes were lysed with ACK lysing buffer (Gibco), followed by two washes with RPMI medium. The following mAbs were used: anti-mouse CD3, CD8α, CD11b, CD69, CD19, CD45, CD107a, GL7, I-A/I-E, interleukin (IL)-2, and TCR β chain from BioLegend; CD4, CD8β, CD40 CD44, CD62L, CD80, CD86, IL-12p40/p70, IFN-γ, and TNF from BD Biosciences; and CD11c, CD45R, CD95, and granzyme B from eBioscience. The CD1d-tetramer was purchased from MBL.

2.5.1 | NK/iNKT cells

After preparation, spleen cells were immediately analyzed via flow cytometry. Cells were incubated with anti-CD16/CD32 (BioLegend) in FACS buffer (PBS with 2% heat-inactivated FBS) for Fc blockade and then stained with surface Abs (CD1d-tetramer/GalCer, anti-TCRVβ-FITC, anti-NK1.1-PE/Cy7, anti-CD69-PE) and viability dye for 30 min on ice. For IFN-γ intracellular staining, after staining with all surface Abs, cells were fixed and permeabilized using the Cytofix/Cytoperm kit (BD Biosciences) and stained with anti-IFN-γ-PE for 30 min at room temperature. After washing, cells were analyzed using a Canto II flow cytometer (BD Bioscience).

2.5.2 | Dendritic cells

Spleen cells were obtained by collagenase D digestion and then incubated with anti-CD16/CD32 in FACS buffer for Fc blockade. Cells were then stained with surface Abs (anti-CD11b-FITC, anti-CD8-APC, anti-CD11c-PE/Cy7, anti-I-AE/K-PB, anti-CD40, anti-CD80, or anti-CD86 biotin) and viability dye for 30 min on ice, followed by incubation with streptavidin-PE. For IL-12 intracellular staining, splenic $CD11c^+$ cells were isolated using CD11c MACS beads (Miltenyi Biotec) for 4 h after aAVC-CoV-2 immunization and then cultured for 2 h in the presence of GolgiPlug (BD Biosciences). After Fc blockade, cells were stained with anti-CD8-APC, anti-CD11c-PE/Cy7, anti-I-A/I-E-PB, and viability dye for 30 min on ice, fixed and permeabilized using the Cytofix/Cytoperm kit (BD Biosciences), and then stained with anti-IL-12p40/p70-PE for 30 min at room

temperature. After washing, cells were analyzed using a Canto II flow cytometer (BD Bioscience).

2.5.3 | B-cells

After preparation, spleen cells were immediately analyzed by flow cytometry. Cells were incubated with anti-CD16/CD32 in FACS buffer for Fc blockade and then stained with surface Abs (anti-B220-FITC, anti-CD95-PE, anti-GL7-APC) and viability dye for 30 min on ice. After washing, cells were analyzed using a Canto II flow cytometer (BD Bioscience).

2.5.4 | T cells

In vivo Ab labeling

To distinguish lung-infiltrating and vascular T cells, mice were injected i.v. with 2 μg of the anti-CD45-APC Ab. After 5 min, mice were euthanized via cervical dislocation, and organs were collected for analysis. Spleen cells and lung MNCs were incubated with anti-CD16/CD32 in FACS buffer for Fc blockade and then stained with surface Abs (anti-CD44-FITC, anti-CD62L-PE, anti-TCRVβ-PB, anti-CD4-BUV737, and anti-CD8-BUV395) and viability dye for 30 min on ice. After washing, the cells were analyzed using Fortessa flow cytometry (BD Bioscience).

Intracellular cytokine staining

To measure antigen-specific T cells, $3–5\times10^6$ lung or spleen cells/well were stimulated with Peptivator SARS-CoV-2 Prot_S Complete (Miltenyi Biotec) in a 96-well U-bottom plate for 16 h in the presence of 2 μg/ml anti-CD28 (BioLegend), 5 μg/ml Alexa488-conjugated anti-CD107a, 5 μg/ml brefeldin A (Sigma-Aldrich), and 2 μM monensin (Sigma-Aldrich), with DMSO used as a negative control. Cells were incubated with anti-CD16/CD32 (BioLegend) in FACS buffer for Fc blockade and then stained with surface antibodies (anti-TCRVβ-PB, anti-CD4-BUV737, anti-CD8-BUV395) and viability dye for 30 min on ice, followed by fixation and permeabilization using the Cytofix/Cytoperm kit (BD Biosciences) and staining with anti-IL-2-PE and anti-TNF-α-PE-Cy7, anti-IFN-γ-APC or -PE, and anti-granzyme B-APC for 30 min at room temperature. After washing, the cells were analyzed using a Foretessa flow cytometer (BD Bioscience).

2.6 | Tumor experiments

C57BL/6 mice were inoculated with 5×10^5 MO4 cells s.c. and then treated with or without 5×10^5 aAVC-OVA or aAVC-OVA/CoV-2 i.v. on day 10. Additionally, C57BL/6 mice were inoculated with 1×10^5 B16 cells s.c. and then treated with or without 5×10^5 aAVC-TRP2 or aAVC-TRP2/CoV-2 i.v. on day 7. Tumor growth was monitored by measuring three perpendicular diameters, and tumor volume was calculated according to the formula $V = L\times W^2\times0.52$, where V is the volume, L is the length, and W is the width.

2.7 | Statistical analysis

Statistical significance was determined at $p<0.05$ using StatMate (3B Scientific). The number of animals (n), median values, and statistical comparison groups are described in the figure legends. All p-values were calculated using Tukey's test for three or more groups or the Mann–Whitney U-test for two groups.

3 | RESULTS

3.1 | Establishment of the whole spike region of aAVC-CoV-2

To establish aAVC-CoV-2, we synthetically generated CoV-2-S genes. After IVT, NIH3T3 cells were both co-transfected with CoV-2-S mRNA and CD1d mRNA and loaded with α-GalCer (Figure 1A). We verified that aAVC-CoV-2 expressed CoV-2-S (mean ± SEM; 1.79 ± 0.13 μg/10^6 cells) using western blot analysis (Figure 1B) and CD1d molecules on the surface using flow cytometry (Figure 1C). Additionally, we confirmed that aAVC-CoV-2 directly stimulated iNKT cells in vitro (Figure 1D).

3.2 | Activation of iNKT and NK cells by administration with aAVC-CoV-2

We then analyzed the innate immune response in vivo using aAVC-CoV-2. B6 mice were injected i.v. with aAVC-CoV-2, and after 16 h, we confirmed that CD1d-tet/Gal$^+$ iNKT cells in the spleen expressed CD69 and produced IFN-γ (Figures 1E and S1A). Simultaneously, NK cells expressed CD69 and produced IFN-γ in wild-type mice but not in CD1d-KO mice (Figures 1F, S1A and S2A). These results suggested that the NK cell adjunctive effect was observed soon after activation of iNKT cells by aAVC-CoV-2. To assess the function of iNKT and NK cells in the spleen, spleen cells of aAVC-CoV-2-injected mice were re-stimulated with or without α-GalCer. We subsequently detected high-IFN-γ-producing spots in immunized mice but not in non-immunized mice (Figure 1G). These findings indicated that aAVC-CoV-2 activated iNKT cells directly and NK cells indirectly.

3.3 | Maturation of endogenous DCs after aAVC-CoV-2 administration

For optimal cross-priming of CTLs against CoV-2-S, the phenotypical maturation of host DCs (e.g., upregulation of co-stimulatory

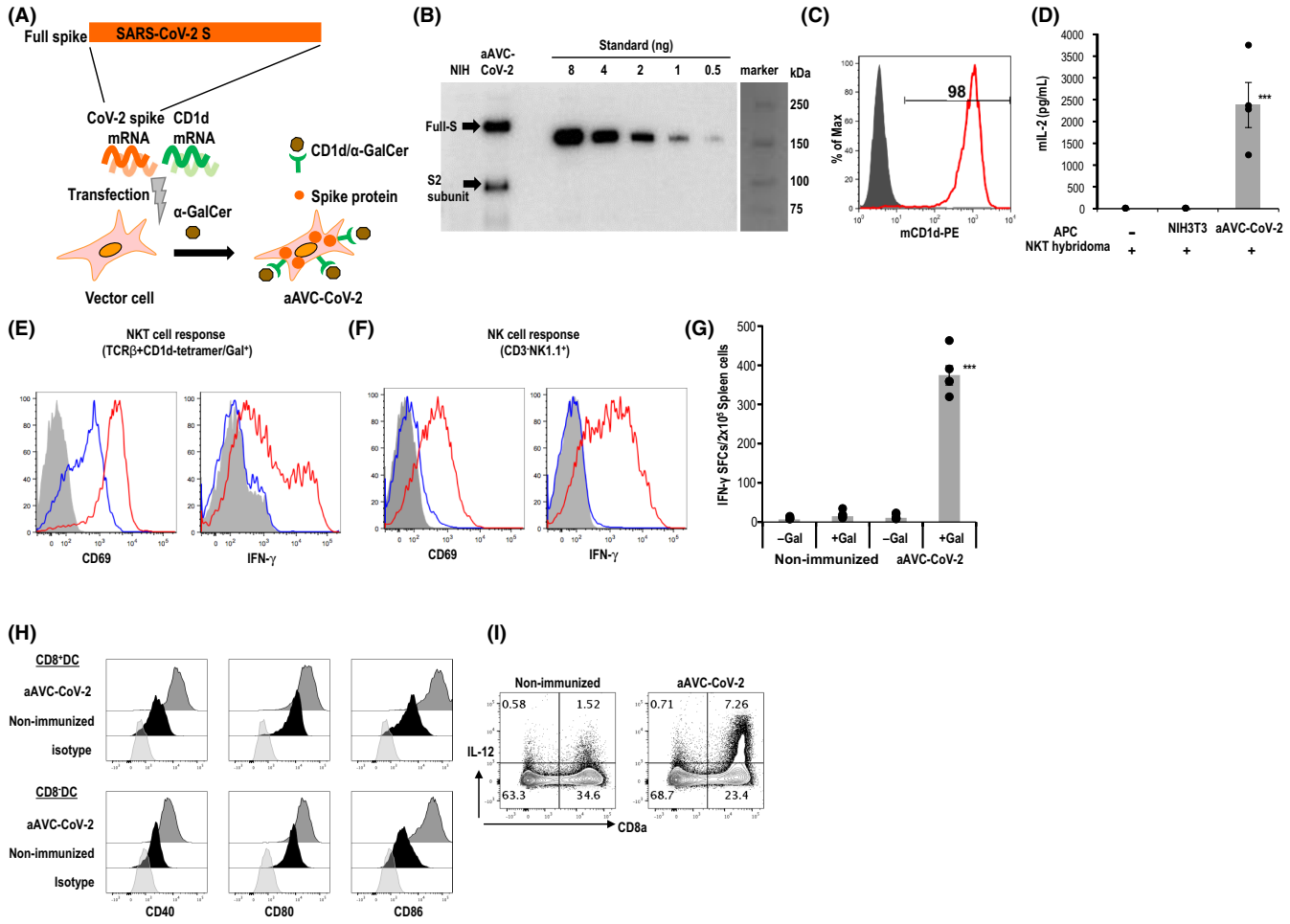

FIGURE 1 aAVC-CoV-2 vaccination elicits an innate immune response. (A) Establishment of aAVC-CoV-2. aAVC-CoV-2 vectors were established using NIH3T3 cells cultured in the presence of α-GalCer and co-electroporation with CoV-2-S and CD1d mRNA. (B, C) Expression levels of CoV-2-S protein and CD1d were assessed by (B) western blot analysis [aAVC-CoV-2 vs. control (NIH3T3)] and (C) flow cytometry for CD1d (red, aAVC-OVA; bold, NIH3T3; shaded, isotype). (D) α-GalCer presentation by aAVC-CoV-2. aAVC-CoV-2 was co-cultured with Vα14 iNKT cell hybridoma 1.2 for 24 h, and IL-2 production in the culture supernatant was evaluated by ELISA (mean ± SEM; $n = 4$). The gray bar and other symbols represent the average and each data point, respectively. $^{***}p < 0.001$, Tukey's test. (E–H) C57BL/6J mice were administered 5×10^5 aAVC-CoV-2 i.v. at day 0. Flow cytometry identified CD69 expression and IFN-γ production by (E) iNKT cells and (F) NK cells in the spleen 16 h after an injection of aAVC-CoV-2 ($n = 4$) (red, aAVC-CoV-2 injected; blue, non-immunized; shaded, isotype). (G) IFN-γ enzyme-linked immune absorbent spot (ELISPOT) assay at day 3. Spleen cells from immunized or non-immunized mice (2×10^5 cells/well) were cultured in the presence or absence of α-GalCer (100 ng/ml) for 16 h, followed by the detection of IFN-γ-producing cells (mean ± SEM; $n = 5$). The gray bar and other symbols represent the average and each data point, respectively. $^{***}p < 0.001$ Tukey's test. (H) Splenic DC maturation. Expression of the co-stimulatory molecules CD40, CD80, and CD86 on splenic DCs was analyzed using flow cytometry 16 h after aAVC-CoV-2 administration ($n = 4$). (I) IL-12 production by splenic DCs. Splenic DCs were harvested 4 h after aAVC-CoV-2 administration, harvested using CD11c MACS beads, and cultured in the presence of GolgiPlug for 2 h. IL-12 production was analyzed using intracellular staining using flow cytometry ($n = 4$)

molecules) and functional maturation of DCs (e.g., IL-12 production) are essential and critical steps for linking innate and adaptive immunity. Initially, we observed that both $CD8a^+$ and $CD8a^-$ subsets of host splenic DCs highly expressed CD40, CD80, and CD86 in wild-type mice at 16 h after administration of aAVC-CoV-2 but not in CD1d-KO mice (Figures 1H, S1B, and S2B). Addition, we confirmed that splenic DCs expressed IL-12 as an indicative marker of functional DCs (Figure 1I). These findings showed that aAVC-CoV-2 caused full maturation of in situ DCs.

3.4 | aAVC-CoV-2 vaccination elicits a Th1-biased Ab response in a $CD4^+$ T-cell-dependent manner

C57BL/6 mice were immunized with aAVC-CoV-2 to evaluate its Ab-producing activity. We observed that the anti-S1 and -S2 subunits of CoV-2-S-specific IgG1 and IgG2b in serum were elevated on days 14, 28, and 56 after immunization (Figure 2A), with the production of the anti-S1 and anti-S2 subunit-specific IgG2 Abs significantly higher than that of the anti-S1 and anti-S2 subunit-specific IgG1 Abs

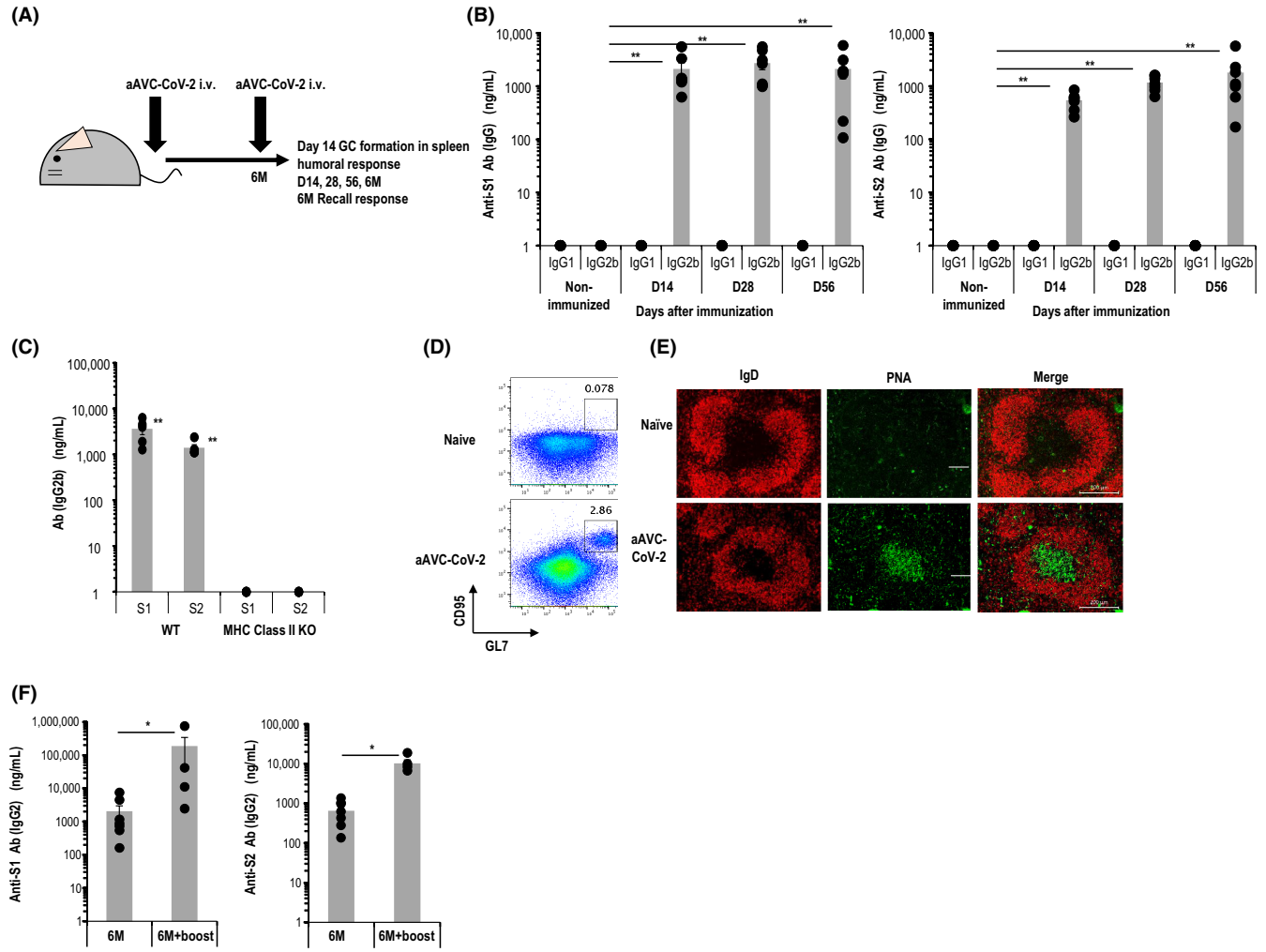

FIGURE 2 aAVC-CoV-2 vaccination elicits an humoral immune response. (A) Schematic diagram of analysis of the humoral response elicited by aAVC-CoV-2. (B–D) C57BL/6J mice were administered 5×10^5 aAVC-CoV-2 i.v. In some experiments, mice were re-challenged with 5×10^5 aAVC-CoV-2 at 6 months later. (B) Anti-CoV-2-S S1 subunit and S2 subunit-specific IgG1 and IgG2b levels were determined using ELISA on days 0, 14, 28, and 56 after aAVC-CoV-2 vaccination (mean ± SEM; $n = 7$). $^{**}p < 0.01$, Mann–Whitney *U*-test. (C) Anti-CoV-2-S S1 subunit and S2 subunit-specific IgG2b levels in wild-type mice vs. MHC Class II-KO mice on day 28 after aAVC-CoV-2 vaccination (mean ± SEM; $n = 5$). $^{**}p < 0.01$ (WT vs. MHC Class II-KO), Mann–Whitney *U*-test. (D, E) GC formation following aAVC-CoV-2 vaccination. After 14 days, (D) GC formation in the spleen was analyzed using flow cytometry using B220-FITC, CD95-PE, and GL7-Alexa678. (E) GC formation in the spleen was verified using fluorescence microscopy using IgD-PE (red) and PNA-Alexa647 (green). Scale bar, 200 μm ($n = 4$). (F) Vaccinated mice were re-administered aAVC-CoV-2 at 6-months later, and the boosting effect on the anti-CoV-2-S S1 subunit and S2 subunit-specific IgG2b level was examined (mean ± SEM; $n = 4$–7). The gray bar and other symbols represent the average and each data point, respectively. $^{*}p < 0.05$, Mann–Whitney *U*-test

(Figure 2B). Additionally, to demonstrate the $CD4^+$ T-cell-dependent Ab response, C57BL/6 or MHC class II-KO mice were immunized with aAVC-CoV-2. We detected Ab production in aAVC-CoV-2-immunized wild-type mice, whereas anti-S1 and anti-S2 subunit-specific IgG2b levels were extremely low in aAVC-CoV-2-immunized MHC class II-KO mice (Figure 2C). These results indicated that aAVC-CoV-2 induced Th1-biased Ab production in mice.

Because germinal center (GC) formation is required for affinity maturation and long-term Ab production,[27] we analyzed the GC response in aAVC-CoV-2-immunized mice. At 14 days after immunization of wild-type mice with aAVC-CoV-2, we detected GC $B220^+CD95^{hi}GL7^{hi}$ B-cells in the spleen using flow cytometry and immunohistochemistry (Figures 2D,E, and S1C). Subsequent examination of the secondary effects of the CoV-2-S-specific Ab revealed that anti-S1 and anti-S2 specific Abs in serum persisted for 6 months after aAVC-CoV-2 immunization (Figure 2F). Moreover, when boosted with aAVC-CoV-2 6 months later, we detected robust Ab production (Figure 2F). These results demonstrated that aAVC-CoV-2 promoted long-term anti-CoV-2-S-specific Ab production and secondary effects.

3.5 | aAVC-CoV-2 vaccination generates antiviral memory CTLs

To assess the generation of CoV-2-S-specific CTL responses, we immunized C57BL/6 mice with aAVC-CoV-2 and analyzed the CTL

response 1 week later. Examination of the T-cell response using in vitro re-stimulation with 15-mer peptide pools for CoV-2-S (Figure 3A) revealed robust expansion of CoV-2-S-specific $CD8^+$ CTLs in the spleen and lung (Figures 3B,D, and S1D), whereas CoV-2-S-specific $CD4^+$ T cells also expanded, but to a lesser extent (Figure 3C,E). Additionally, both $CD4^+$ and $CD8^+$ T cells displayed the production of multiple cytokines (IFN-γ, TNF-α, and IL-2) in response to antigen stimulation. In particular, lung $CD8^+$ T cells showed high levels of cytotoxic molecules, granzyme B, and CD107a (Figure 3F). These findings suggested that aAVC-CoV-2 promoted an antigen-specific multifunctional T-cell response. Moreover, we detected memory $CD4^+$ and $CD8^+$ T cells in the lungs 6 months after aAVC-CoV-2 immunization and identified a clear boosting effect of antigen-specific $CD4^+$ and $CD8^+$ T-cell immunity as a secondary response (Figures 3G and S3). This finding confirmed that aAVC-CoV-2 immunization established CoV-2-S-specific memory $CD4^+$ and $CD8^+$ T cells.

We then determined whether vaccine-induced T cells infiltrated the lung parenchyma by performing i.v. labeling with the anti-CD45 antibody to differentiate between tissue-infiltrating ($CD45^-$) and circulating ($CD45^+$) lung $CD4^+$ and $CD8^+$ T cells (Figure 4A). In the aAVC-CoV-2-treated group, we found that the tissue-infiltrating

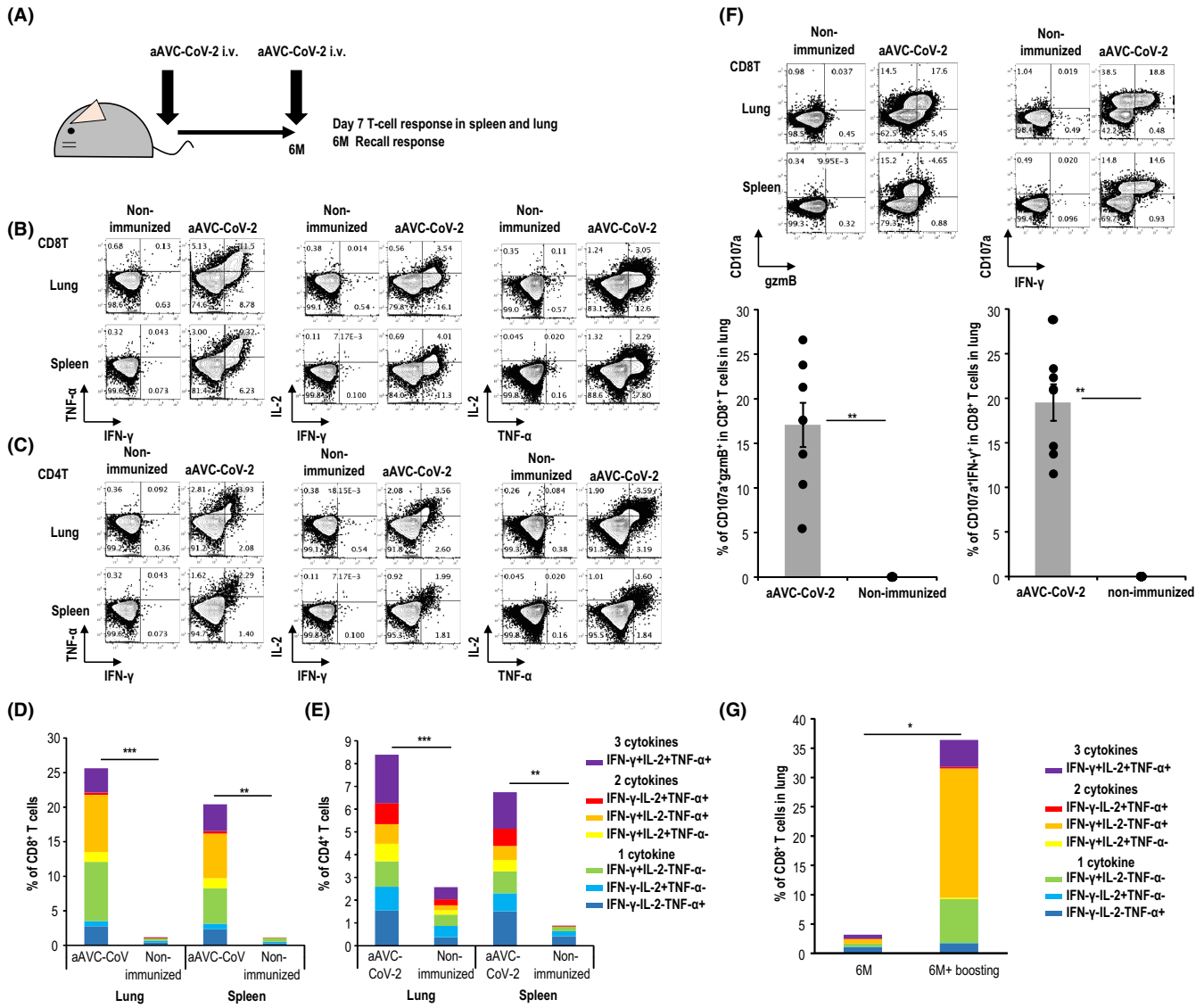

FIGURE 3 aAVC-CoV-2 vaccination elicits an antigen-specific T-cell response. (A) Schematic diagram of analysis of the T-cell response elicited by aAVC-CoV-2. C57BL/6J mice were administered 5×10^5 aAVC-CoV-2 i.v. In some experiments, mice were re-challenged with 5×10^5 aAVC-CoV-2 at 6-months later. Spleens and lungs were harvested and stimulated with CoV-2-S peptide pools. (B, D) $CD8^+$ and (C, E) $CD4^+$ T cells were analyzed for cytokine production using intracellular staining at day 7 after immunization (mean; $n = 7$–10/group). $^{**}p < 0.01$, $^{***}p < 0.001$, Mann–Whitney *U*-test. (F) Analysis of $CD8^+$ T cells for the cytolytic markers granzyme B and CD107a (left) or IFN-γ and CD107a (right) (mean ± SEM; $n = 7$–8/group). The gray bar and other symbols represent the average and each data point, respectively. $^{**}p < 0.01$, Mann–Whitney *U*-test. (G) Recall response of CoV-2-S-specific $CD8^+$ T-cell response. At 6 months after initial immunization, mice were re-challenged with aAVC-CoV-2 and, 7 days later, lung $CD8^+$ T cells were analyzed using flow cytometry (mean; $n = 4$). The gray bar and other symbols represent the average and each data point, respectively. $^*p < 0.05$, Mann–Whitney *U*-test

population was increased between both lung $CD8^+$ and $CD4^+$ T cells (Figure 4B,C), with most of this population an effector/effector memory subset ($CD44^+CD62L^-$; Figure 4D,E). In fact, we identified infiltration of lymphocytes ($CD4^+$ and $CD8^+$ T cells) along with $CD11c^+$ cells into parenchymal tissue around blood vessels in lungs from immunized mice (Figure 4F). These findings confirmed the infiltration of vaccine-induced effector/effector memory subsets in lung parenchyma.

3.6 | Establishment of an antitumor model while maintaining anti-SARS-CoV-2 viral potential using dual antigen-expressing aAVCs

Because cancer patients are often immunocompromised, they are susceptible to SARS-CoV-2 infection, therefore treatments demonstrating high efficacy against cancer, while also maintaining antiviral capacity, would be a critically important strategy for cancer patients. Because the present results showed that aAVC-CoV-2 induced long-term CTL induction (Figures 3Gand S3), we attempted to establish a dual antigen-expressing aAVC for the induction of antitumor CTLs together with the prevention of SARS-CoV-2. For this purpose, we evaluated antitumor responses using aAVCs co-expressing OVA antigen or TAA together with the CoV-2-S antigen (Figures 5A). Initially, we examined the $CD8^+$ T-cell response to CoV-2-S and OVA in mice administered aAVCs expressing both antigens (aAVC-OVA/CoV-2), as well as in vitro re-stimulation with peptide pools of CoV-2-S or OVA protein, respectively, at day 7 post-immunization (Figure 5B,C). We then assessed the antitumor effects of dual antigen-expressing aAVCs. Comparison of the therapeutic effect of aAVC-OVA/CoV-2 and aAVC-OVA against MO4 (OVA-expressing B16 melanoma) revealed similar antitumor effects (Figure 5B,D). Additionally, we established aAVC-TRP2/CoV-2 and aAVC-TRP2 using a real melanoma antigen and then compared their respective therapeutic effects against B16 melanoma. As shown in Figure 5E, we observed a similar sufficient therapeutic effect for both aAVC-TRP2 and aAVC-TRP2/CoV-2. Furthermore, immunohistochemistry analysis of the trafficking of $CD8^+$ T cells revealed many $CD8^+$ T cells (but fewer $CD4^+$ T cells) located close to $CD31^+$ tumor vessels along with $CD11c^+$ DCs in aAVC-injected mice but not in untreated mice (Figures 5F,G, and S4). These results demonstrated that aAVC-TAA/CoV-2 and aAVC-TAA could not only induce a $CD8^+$ T-cell response against tumors and SARS-CoV-2 but also elicit an antitumor therapeutic effect (Figure S5).

4 | DISCUSSION

For complete elimination of latent virus, a strong CTL response in addition to neutralizing Abs is required. In this study, we demonstrated that the aAVC-CoV-2 vaccine generated multifunctional CoV-2-S-antigen-specific $CD4^+$ and $CD8^+$ T cells by promoting full maturation of in situ DCs via long-term iNKT cell activation as memory T cells in addition to Th1-biased Ab production. Previous reports showed that vaccination using CoV-2-S mRNA (~1 μg/mouse, two immunizations) sufficiently protected against viral replication in a murine model.[28–30] To show the T-cell immune responses, another group reported the levels of CoV-2-S-antigen-specific IFN-γ-producing $CD4^+$ T and $CD8^+$ T cells at the effector phase at ~0.6% and 4.5% of total $CD4^+$ and $CD8^+$ T cells, respectively, in the lungs of mice vaccinated with 30 μg mRNA/mouse.[31] In the present study, we demonstrated levels of CoV-2-S-antigen-specific IFN-γ-producing $CD4^+$ T cells and $CD8^+$ T cells at 8% and 25% of total $CD4^+$ and $CD8^+$ T cells, respectively, in the lungs of mice vaccinated with aAVC-CoV-2 (3 μg of CoV-2-S mRNA; Figure 4). Our results showed that vaccination with aAVC-CoV-2 harboring a 10-fold lower amount of CoV-2-S mRNA resulted in the generation of up to 10-fold higher levels of antigen-specific $CD4^+$ or $CD8^+$ T cells relative to the currently used mRNA vaccine. Moreover, this suggests that, although mRNA vaccines for SARS-CoV-2 can induce $CD8^+$ CTLs,[28,31] aAVC-CoV-2 induced the generation of higher numbers of CTLs that were not only capable of producing multiplex cytokines (Figure 4) but also demonstrating high-frequency infiltration of the lungs of vaccinated mice. This is particularly beneficial, because SARS-CoV-2 initially infects the lungs. In fact, we observed that CTLs were maintained in the lung for at least 6 months as long-term memory CTLs that were capable of being robustly boosted. Because the lifespan of mice is ~1 to ~2 years, CTLs against SARS-CoV-2 could potentially persist for considerable periods in humans. This implies that a single vaccination could elicit memory CTLs and $CD4^+$ T-cell-mediated Ab production. Therefore, aAVC-CoV-2 could be beneficial as a second-line treatment for patients who may be resistant to current vaccines and members of a high-risk group.

FIGURE 4 aAVC-CoV-2 promotes T-cell infiltration in the lungs of vaccinated mice. (A) Schematic illustration of the T-cell response elicited by aAVC-CoV-2 in the lungs of vaccinated mice. To distinguish between tissue-infiltrating cells and circulating cells in the lung vasculature, mice were injected i.v. with 2 μg anti-CD45-APC Ab, and lungs were collected after 5 min. Lung $CD4^+$ and $CD8^+$ T-cell subsets were analyzed using flow cytometry. Representative flow cytometry data of lung (B, left; D left) $CD8^+$ T cells and (C, left; E, left) $CD4^+$ T cells in non-immunized or aAVC-CoV-2-immunized mice (day 7). Data show the proportion of $CD45^+$ (circulating) and $CD45^-$ (tissue-infiltrating) cells between (B, right) $CD8^+$ T cells and (C, right) $CD4^+$ T cells. The proportion of $CD45^+CD44^{hi}CD62L^-$ (circulating effector/effector memory) and $CD45^-CD44^{hi}CD62L^-$ (infiltrating effector/effector memory) cells in lung (D, right) $CD8^+$ T cells or (E, right) $CD4^+$ T cells (mean ± SEM; $n = 8$) The gray bar and other symbols represent the average and each data point, respectively. $^{**}p < 0.01$, Mann–Whitney *U*-test. (F) Representative H&E staining and immunohistochemistry staining of lung tissues. The sections of mouse lung tissues were stained with H&E (right) and examined under a microscope (original magnification, ×20). For immunohistochemistry, lung tissues were stained with CD11c (blue), CD31 (green), and CD8 (red) or CD4 (red). Images are representative of four experiments. Scale bar, 100 μm

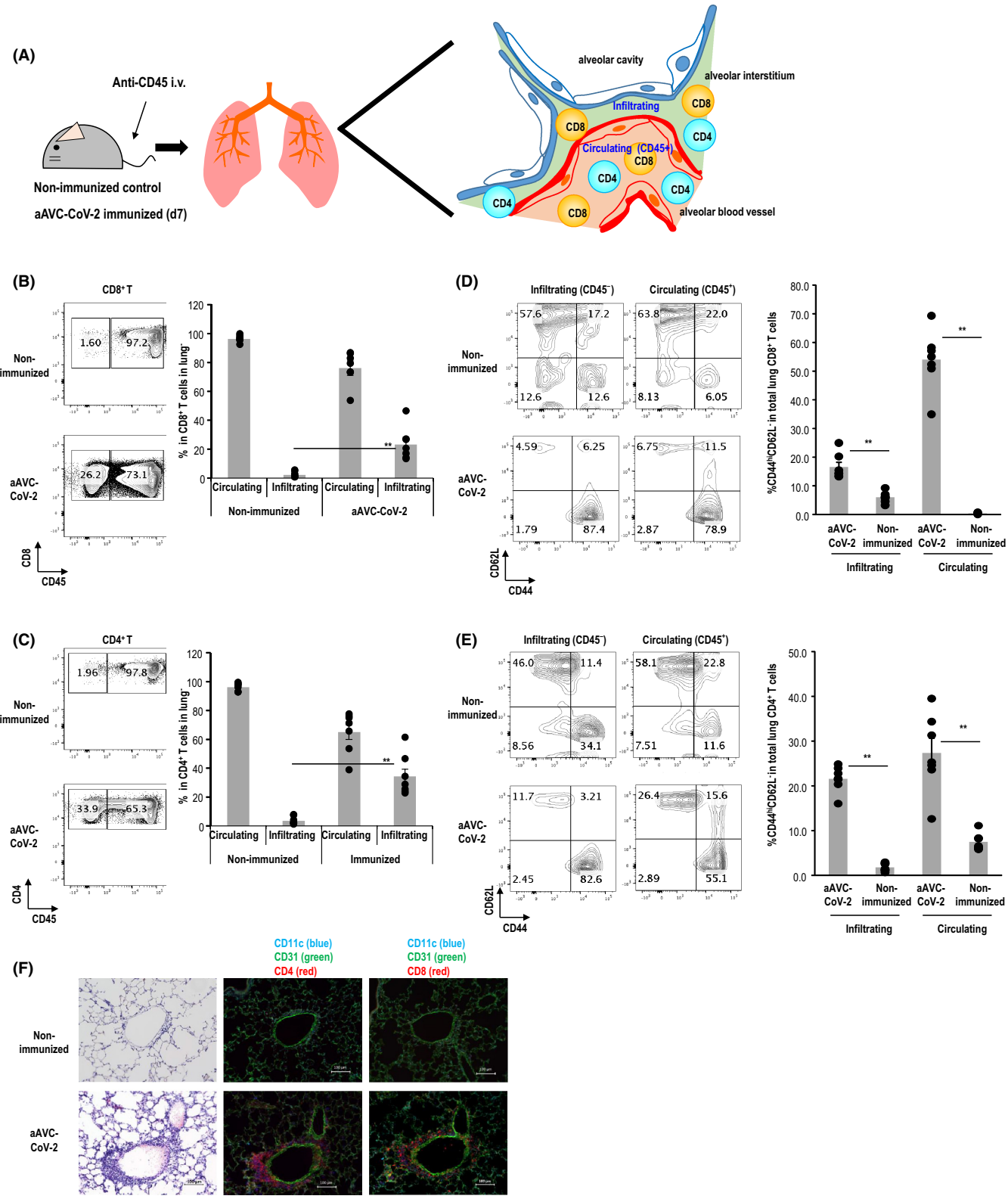

Furthermore, we showed that aAVC-TAA/CoV-2 elicited both an antitumor effect together with protection against SARS-CoV-2. Fatality in cancer patients suffering from COVID-19 is substantially higher than that of healthy individuals.[32–37] Additionally, studies report chronic viral persistence and shedding of SARS-CoV-2 in immunocompromised patients, reporting the emergence of mutated variants.[38,39] Moreover, patients with solid tumors and vaccinated against COVID-19 do not show Ab production until receiving a second dose.[40] Furthermore, in B-cell malignancies, such as chronic lymphocytic leukemia and multiple myeloma, Ab titers remain low, even after the second vaccine dose.[41,42] Cancer progression or chemotherapy can also increase the risk of infection for cancer patients;

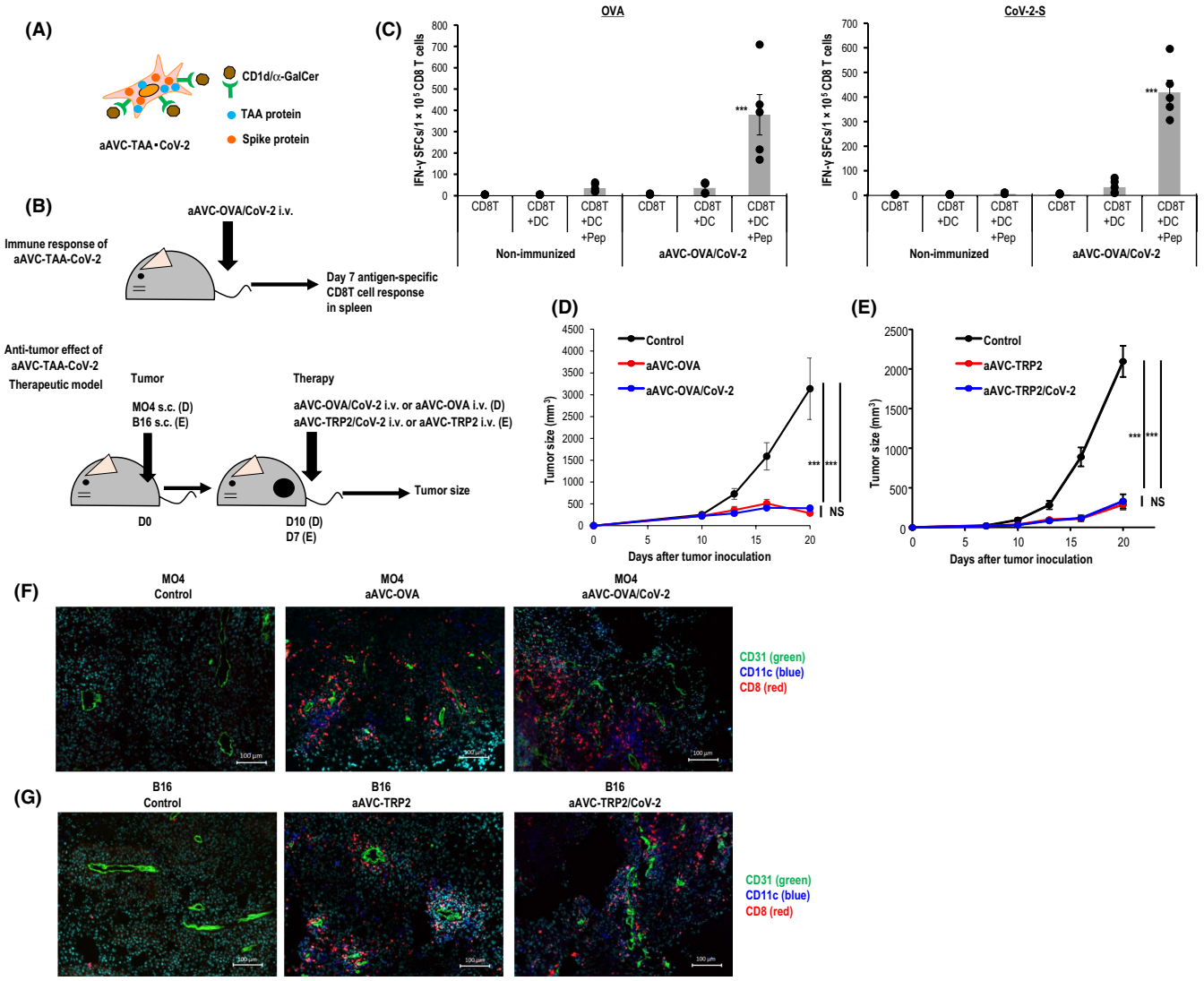

FIGURE 5 Antigen-specific $CD8^+$ T-cell response and the antitumor effect of multivalent aAVC-TAA/CoV-2. (A) aAVC-TAA/CoV-2 expresses TAA (OVA or TRP2) and CoV-2-S protein inside cells and the CD1d/α-GalCer complex on the cell surface. (B) Schematic illustration of the (C) T-cell response and (D, E) antitumor responses elected by aAVC-TAA/CoV-2. (C) C57BL/6J mice were administered 5×10^5 aAVC-OVA/CoV-2 i.v. (left). On day 7, OVA-specific $CD8^+$ T-cell (left) and CoV-2-S-specific $CD8^+$ T-cell (right) responses were evaluated using IFN-γ ELISPOT assay after culturing with protein or peptide pools for 24 h (mean ± SEM; $n = 5$). The gray bar and other symbols represent the average and each data point, respectively. ***$p < 0.001$, Tukey's test. (D) The antitumor effect of aAVC-OVA/CoV-2. Mice were inoculated with 5×10^5 MO4 s.c. and treated with 5×10^5 aAVC-OVA/CoV-2 or aAVC-OVA i.v. 10-days later, after which tumor size was measured (mean ± SEM; $n = 6$–7/group) ***$p < 0.001$, Tukey's test. (E) Antitumor effect by aAVC-TRP2/CoV-2. Mice were inoculated with 1×10^5 B16 s.c. and treated with 5×10^5 aAVC-TRP2/CoV-2 or aAVC-TRP2 i.v. on day 7. Tumor size was measured (mean ± SEM, $n = 6$–7/group). ***$p < 0.001$, Tukey's test. (F, G) Representative immunohistochemistry staining of tumor tissues (F) MO4 and (G) B16 harvested 7–10 days after aAVC treatment. The sections of tumor tissues were stained with CD11c (blue), CD31 (green), and CD8 (red). Images are representative four experiments. Scale bar, 100 μm. NS, not significant

therefore, a second-line vaccine capable of inducing a robust and durable CTL response against both SARS-CoV-2 and tumors for these high-risk groups is warranted. The aAVC-TAA/CoV-2 vaccine presented here showed promising efficacy in murine preclinical models as a specialized vaccine for cancer patients.

In summary, we demonstrated that the potential efficacy of the aAVC-CoV-2 vaccine as prophylactic immunotherapy and a novel SARS-CoV-2 vaccine, particularly for high-risk patients. We detected T-cell responses in the lungs of vaccinated mice, highlighting the potential protective role of lung-homing T cells against SARS-CoV-2. Subsequent evaluation of vaccination with dual antigen-expressing aAVC-TAA/CoV-2 revealed both antiviral and antitumor efficacy. Future studies dual antigen-expressing aAVC are warranted to demonstrate the function of each type of generated CTL and elucidate the precise mechanisms associated with multivalent aAVC platforms as cancer therapeutic vaccines, as well as preventive COVID-19 vaccines. These results illustrate the potential of these vaccines as candidates with beneficial features for future application and development.

ACKNOWLEDGMENTS

We thank Ms. Sanpei and Ms. Aoshima for their support with the murine experiments and Dr. Nakazato and Ms. Kurokochi for their help with the molecular experiments.

DISCLOSURE

The authors declare no competing interests.

ETHICS STATEMENT

This study was approved by the Institutional Animal Care and Use Committee and carried out according to RIKEN guidelines.

ORCID

Shin-ichiro Fujii https://orcid.org/0000-0003-3586-3976

REFERENCES

1. Cucinotta D, Vanelli M. WHO declares COVID-19 a pandemic. *Acta Biomed*. 2020;91(1):157-160.
2. Polack FP, Thomas SJ, Kitchin N, et al. Safety and efficacy of the BNT162b2 mRNA Covid-19 vaccine. *N Engl J Med*. 2020;383(27):2603-2615.
3. Baden LR, El Sahly HM, Essink B, et al. Efficacy and safety of the mRNA-1273 SARS-CoV-2 vaccine. *N Engl J Med*. 2021;384(5):403-416.
4. Bange EM, Han NA, Wileyto P, et al. CD8(+) T cells contribute to survival in patients with COVID-19 and hematologic cancer. *Nat Med*. 2021;27(7):1280-1289.
5. Swadling L, Diniz MO, Schmidt NM, et al. Pre-existing polymerase-specific T cells expand in abortive seronegative SARS-CoV-2. *Nature*. 2021;601(7891):110-117.
6. Schulien I, Kemming J, Oberhardt V, et al. Characterization of pre-existing and induced SARS-CoV-2-specific CD8(+) T cells. *Nat Med*. 2021;27(1):78-85.
7. Ferretti AP, Kula T, Wang Y, et al. Unbiased screens show CD8(+) T cells of COVID-19 patients recognize shared epitopes in SARS-CoV-2 that largely reside outside the spike protein. *Immunity*. 2020;53(5):1095-1107.
8. Sekine T, Perez-Potti A, Rivera-Ballesteros O, et al. Robust T cell immunity in convalescent individuals with asymptomatic or mild COVID-19. *Cell*. 2020;183(1):158-168.
9. Grifoni A, Weiskopf D, Ramirez SI, et al. Targets of T cell responses to SARS-CoV-2 coronavirus in humans with COVID-19 disease and unexposed individuals. *Cell*. 2020;181(7):1489-1501.
10. Braun J, Loyal L, Frentsch M, et al. SARS-CoV-2-reactive T cells in healthy donors and patients with COVID-19. *Nature*. 2020;587(7833):270-274.
11. Mateus J, Grifoni A, Tarke A, et al. Selective and cross-reactive SARS-CoV-2 T cell epitopes in unexposed humans. *Science*. 2020;370(6512):89-94.
12. Mallajosyula V, Ganjavi C, Chakraborty S, et al. CD8(+) T cells specific for conserved coronavirus epitopes correlate with milder disease in COVID-19 patients. *Sci Immunol*. 2021;6(61):eabg5669.
13. Shimizu K, Iyoda T, Sanpei A, et al. Identification of TCR repertoires in functionally competent cytotoxic T cells cross-reactive to SARS-CoV-2. *Commun Biol*. 2021;4(1):1365.
14. Lineburg KE, Grant EJ, Swaminathan S, et al. CD8(+) T cells specific for an immunodominant SARS-CoV-2 nucleocapsid epitope cross-react with selective seasonal coronaviruses. *Immunity*. 2021;54:1055-1065.
15. Nelde A, Bilich T, Heitmann JS, et al. SARS-CoV-2-derived peptides define heterologous and COVID-19-induced T cell recognition. *Nat Immunol*. 2021;22(5):74-85.
16. Kared H, Redd AD, Bloch EM, et al. SARS-CoV-2-specific CD8+ T cell responses in convalescent COVID-19 individuals. *J Clin Invest*. 2021;131(5):e145476.
17. Fujii S, Shimizu K, Smith C, Bonifaz L, Steinman RM. Activation of natural killer T cells by a-galactosylceramide rapidly induces the full maturation of dendritic cells *in vivo* and thereby acts as an adjuvant for combined CD4 and CD8 T cell immunity to a coadministered protein. *J Exp Med*. 2003;198(2):267-279.
18. Fujii S, Liu K, Smith C, Bonito AJ, Steinman RM. The linkage of innate to adaptive immunity via maturing dendritic cells in vivo requires CD40 ligation in addition to antigen presentation and CD80/86 costimulation. *J Exp Med*. 2004;199(12):1607-1618.
19. Fujii S, Goto A, Shimizu K. Antigen mRNA-transfected, allogeneic fibroblasts loaded with NKT-cell ligand confer antitumor immunity. *Blood*. 2009;113(18):4262-4672.
20. Shimizu K, Mizuno T, Shinga J, et al. Vaccination with antigen-transfected, NKT cell ligand-loaded, human cells elicits robust in situ immune responses by dendritic cells. *Cancer Res*. 2013;73(1):62-73.
21. Shimizu K, Yamasaki S, Shinga J, et al. Systemic DC activation modulates the tumor microenvironment and shapes the long-lived tumor-specific memory mediated by CD8+ T cells. *Cancer Res*. 2016;76(13):3756-3766.
22. Fujii S, Shimizu K. Exploiting antitumor immunotherapeutic novel strategies by deciphering the cross-talk between invariant NKT cells and dendritic cells. *Front Immunol*. 2017;8:886.
23. Fujii S, Shimizu K. Immune networks and therapeutic targeting of iNKT cells in cancer. *Trends Immunol*. 2019;40(11):984-997.
24. Yamasaki S, Shimizu K, Kometani K, Sakurai M, Kawamura M, Fujii S. *In vivo* dendritic cell targeting cellular vaccine induces CD4(+) Tfh cell-dependent antibody against influenza virus. *Sci Rep*. 2016;6:35173.
25. Mendiratta SK, Martin WD, Hong S, Boesteanu A, Joyce S, Van Kaer L. CD1d1 mutant mice are deficient in natural T cells that promptly produce IL-4. *Immunity*. 1997;6(4):469-477.
26. Shimizu K, Kurosawa Y, Taniguchi M, Steinman RM, Fujii S. Murine NKT hybridoma. *J Exp Med*. 2007;204(11):2641-2653.
27. MacLennan IC. Germinal centers. *Annu Rev Immunol*. 1994;12:117-139.
28. Corbett KS, Edwards DK, Leist SR, et al. SARS-CoV-2 mRNA vaccine design enabled by prototype pathogen preparedness. *Nature*. 2020;586(7830):567-571.
29. DiPiazza AT, Leist SR, Abiona OM, et al. COVID-19 vaccine mRNA-1273 elicits a protective immune profile in mice that is not associated with vaccine-enhanced disease upon SARS-CoV-2 challenge. *Immunity*. 2021;54(8):1869-1882.
30. Ji RR, Qu Y, Zhu H, et al. BNT162b2 vaccine encoding the SARS-CoV-2 P2 S protects transgenic hACE2 mice against COVID-19. *Vaccines (Basel)*. 2021;9(4):324.
31. Laczko D, Hogan MJ, Toulmin SA, et al. A single immunization with nucleoside-modified mRNA vaccines elicits strong cellular and humoral immune responses against SARS-CoV-2 in mice. *Immunity*. 2020;53(4):724-732.
32. Tian J, Yuan X, Xiao J, et al. Clinical characteristics and risk factors associated with COVID-19 disease severity in patients with cancer in Wuhan, China: a multicentre, retrospective, cohort study. *Lancet Oncol*. 2020;21(20):893-903.
33. Mehta V, Goel S, Kabarriti R, et al. Case fatality rate of cancer patients with COVID-19 in a New York hospital system. *Cancer Discov*. 2020;10(7):935-941.
34. Lunski MJ, Burton J, Tawagi K, et al. Multivariate mortality analyses in COVID-19: comparing patients with cancer and patients without cancer in Louisiana. *Cancer*. 2021;127(2):266-274.
35. Ruthrich MM, Giessen-Jung C, Borgmann S, et al. COVID-19 in cancer patients: clinical characteristics and outcome-an analysis of the LEOSS registry. *Ann Hematol*. 2021;100(2):383-393.

36. Passamonti F, Cattaneo C, Arcaini L, et al. Clinical characteristics and risk factors associated with COVID-19 severity in patients with haematological malignancies in Italy: a retrospective, multicentre, cohort study. *Lancet Haematol*. 2020;7(10):e737-e745.
37. Bhogal T, Khan UT, Lee R, et al. Haematological malignancy and nosocomial transmission are associated with an increased risk of death from COVID-19: results of a multi-center UKcohort. *Leuk Lymphoma*. 2021;62(7):1682-1691.
38. Choi B, Choudhary MC, Regan J, et al. Persistence and evolution of SARS-CoV-2 in an immunocompromised host. *N Engl J Med*. 2020;383(23):2291-2293.
39. Kemp SA, Collier DA, Datir RP, et al. SARS-CoV-2 evolution during treatment of chronic infection. *Nature*. 2021;592(7853):277-282.
40. Massarweh A, Eliakim-Raz N, Stemmer A, et al. Evaluation of seropositivity following BNT162b2 messenger RNA vaccination for SARS-CoV-2 in patients undergoing treatment for cancer. *JAMA Oncol*. 2021;7(8):1133-1140.
41. Pimpinelli F, Marchesi F, Piaggio G, et al. Fifth-week immunogenicity and safety of anti-SARS-CoV-2 BNT162b2 vaccine in patients with multiple myeloma and myeloproliferative malignancies on active treatment: preliminary data from a single institution. *J Hematol Oncol*. 2021;14(1):81.
42. Herishanu Y, Avivi I, Aharon A, et al. Efficacy of the BNT162b2 mRNA COVID-19 vaccine in patients with chronic lymphocytic leukemia. *Blood*. 2021;137(23):3165-3173.

SUPPORTING INFORMATION

Additional supporting information may be found in the online version of the article at the publisher's website.

How to cite this article: Shimizu K, Ueda S, Kawamura M, Satoh M, Fujii S-i. A single immunization with cellular vaccine confers dual protection against SARS-CoV-2 and cancer. *Cancer Sci*. 2022;113:2536-2547. doi: 10.1111/cas.15434